energies

MDPI

Article

Numerical Modeling and Simulation of a Spark-Ignition Engine Fueled with Ammonia-Hydrogen Blends

Gabriele D'Antuono, Davide Lanni *, Enzo Galloni and Gustavo Fontana *

Department of Civil and Mechanical Engineering, University of Cassino and Southern Latium, 03043 Cassino, Italy

* Correspondence: davide.lanni@unicas.it (D.L.); fontana@unicas.it (G.F.)

Abstract: Carbon-free fuels, in particular ammonia and hydrogen, could play a significant role in the decarbonization of the mobility sector. In this work, the authors assessed the operation of a light-duty spark-ignition engine fueled with an ammonia–hydrogen blend (85% ammonia and 15% hydrogen by volume) using a 1D predictive model. Three-dimensional computations have been used in order to verify the reliability of the 1D model. The addition of hydrogen to the air–fuel mixture allows the operating capacity of the engine to be extended with respect to neat ammonia fueling. The engine can be properly regulated between 1500 rpm and 3000 rpm. Its operating range reduces as engine speed increases, and it cannot run at 6000 rpm. This is due to different engine operating constraints being exceeded. The maximum engine torque is about 240 Nm and is reached at 1500 rpm. The engine efficiency ranges between 42% and 19%, and the specific fuel consumption varies from about 350 g/kWh to about 750 g/kWh. The results provide both performances and operating ranges of the engine allowing us to define optimized engine maps obtained by means of a constrained optimization.

Keywords: ammonia; hydrogen; carbon-free fuels; e-fuels; SI engines; downsizing

Citation: D'Antuono, G.; Lanni, D.; Galloni, E.; Fontana, G. Numerical Modeling and Simulation of a Spark-Ignition Engine Fueled with Ammonia-Hydrogen Blends. *Energies* **2023**, *16*, 2543. https://doi.org/10.3390/en16062543

Academic Editors: Roberta De Robbio and Maria Cristina Cameretti

Received: 10 February 2023
Revised: 2 March 2023
Accepted: 6 March 2023
Published: 8 March 2023

1. Introduction

Today, in terms of the pollutant emissions of the Internal Combustion Engines (ICEs) complying with the current regulations, we can affirm that these engines have won the battle against those emissions that are considered to be harmful for the human health. However, the emissions of greenhouse gases, deriving from the combustion of traditional fossil fuels, still require significant attention.

In order to drastically reduce CO_2 emissions, the only effective solution is to find new carbon-free fuels.

As carbon-free fuels, ammonia [1–3] and hydrogen [4–6] represent good choices as fuels for ICEs. Furthermore ammonia can be used as a raw material to produce hydrogen [7,8].

The combustion characteristics of ammonia are very different from those of hydrogen and gasoline, and in Table 1, a brief summary of these is reported.

Table 1. Ammonia properties vs. gasoline and hydrogen properties [2,9,10].

	Ammonia	Gasoline	Hydrogen
Storage	Liquid (300 K–11 bar)	Liquid (300 K–1 bar)	Compressed (300 K, 700 bar)
LHV (MJ/kg)	18.8	44.5	120
Stoichiometric air to fuel ratio (-)	6.05	14.8	34.3
Heat released by a volume unit of stoichiometric air-fuel mixture (MJ/m^3)	2.81	3.46	2.88
Laminar burn velocity (m/s) at ambient condition	0.015	0.58	3.51
Octane number	130	92–98	>130
Auto-ignition temperature (K)	930	503	503
Explosion limit (% volume ratio)	16–28	1.4–1.6	4.5–75
Density (kg/m^3)	0.703	740	0.082

Ammonia clearly shows the worst combustion characteristics compared to hydrogen and gasoline: its laminar flame speed is 57% less than that of gasoline and 98% less than hydrogen; ammonia's LHV is much smaller than the LHVs of both gasoline and hydrogen. This suggests that ammonia is better to use in blends [11]. However, at present, neat ammonia, as a fuel for ICEs, is also under study.

In [12], the authors focused their attention on the performance of a spark-ignition engine fueled with neat ammonia. By means of 1D-3D analyses, they investigated the influence of boost pressure, load conditions and spark timing on the behavior of the engine running with ammonia. In the end, they found out that ammonia drastically reduces the typical operation map of a light-duty SI engine. However, ammonia could be effectively used in engines running at low–medium speeds, preferably featuring high pressure ratios.

Scharl et al. [13] investigated the mixture formation and spray combustion on a rapid compression–expansion machine. Combining 1D analyses and optical investigations, they found out that ammonia flames do not appear stable after ignition. Considering ammonia spray, the authors reported that close to the nozzle, the temperatures are low and the equivalence ratio drops below 1. Cui et al. [14] experimentally analyzed the effect of a pre-chamber with a jet flame in order to improve the ignition phase of ammonia and its combustion. They found that increasing the pre-chamber volume leads to an increase in jet duration and ignition energy.

Ammonia can also be added to conventional fuels such as diesel or gasoline. El Fattah et al. [15] analyzed the emissions of a spark-ignition engine powered by water ammonia–gasoline blends. In particular, using this blend, they obtained a higher engine thermal efficiency, but also a higher amount of NO_x.

In [16], Zhang et al. experimentally investigated the performance of a two-stroke low-speed engine powered by a dual-fuel direct injection mixture composed by ammonia and diesel. Varying the ammonia's amount, they discovered that diesel injection timing helps the regulation of the ignition and early stage of combustion. The authors also pointed out that this solution is important for the reduction in ammonia's combustion duration, and, consequently, the indicated thermal efficiency increases.

Nowadays, ammonia–hydrogen blends are objects of study. In particular, in [17], a numerical study on the combustion characteristics of a spark-ignition engine fueled by ammonia and hydrogen which is obtained from the reformation of the exhaust gas is presented. The authors found that by adding hydrogen, up to 10% by volume, the in-cylinder pressure increased, and the combustion duration decreased, leading to an improvement in combustion and thermal efficiencies.

In [18], Lhuillier et al. experimentally investigated the combustion of ammonia–hydrogen blends in spark-ignition engines. They considered a constant engine speed equal to 1500 rpm, an intake pressure between 0.1 and 0.12, an equivalence ratio ranging from 0.6 to 1.2, and a fraction of hydrogen in the fuel mixture varying from 0 to 0.15 by mass. They found out that adding hydrogen also makes the engine run in lean operations with a COV_{IMEP} less than 5%. In this way, hydrogen allows an improvement in stability and performance as well, since the combustion duration decreases at a high rate until the H_2 percentage is less than 20% (volume basis); over this threshold, the decrease slows down.

Frigo et al. [19] experimentally investigated a spark-ignition engine, used as a range extender for electric vehicles, powered by ammonia and hydrogen where hydrogen is obtained by ammonia. After defining the type of injector and its timings, they considered either full-load operations or half-load conditions, with the engine running from 2500 rpm to 5000 rpm and stoichiometric mixtures. The authors showed the amount of hydrogen necessary to increase the combustion velocity mainly depends on load and less on engine speed, and, in particular, they considered a percentage of hydrogen of 6% (volume basis) at full load and 10% at partial load.

In [20], there is a numerical study on the ammonia–hydrogen blends' combustion characteristics compared to methane, methanol, and ethanol combustion. Using a 1D approach, the authors observed several engine conditions by varying the equivalence ratio

(from 0.7 to 1.3), the hydrogen mole fraction (from 0 to 100%), and the compression ratio. They found out that the laminar burning velocity needs an amount of 40–70% of hydrogen in order to reach the same level of hydrocarbon fuels unless the compression ratio increases. The ignition energy shows an opposite trend to laminar burning velocity. The authors also found that due to an incomplete oxidation, the combustion efficiency decreases if the amount of hydrogen and the equivalence ratio increase.

Pyrc et al. [21] experimentally investigated an SI engine characterized by a variable pressure ratio and modified it in order to work as a dual-fuel engine fueled with ammonia and hydrogen. Considering two different pressure ratios (8 and 10) and an amount of the energy shared by hydrogen from 0 to 70%, the results show that with 12% of energy shared by hydrogen, the instability related to the ignition process disappears. In particular, with a compression ratio equal to 8, the authors observed that ignition delay decreases two times, while for a compression ratio equal to 10, it decreases almost three times; naturally, the specific energy consumption decreases as the compression ratio increases.

Due to the low engine speeds that characterize the heavy-duty engines, ammonia could effectively be fired in applications such as marine engines, as reported in [22,23]. In addition, in [24], the authors theoretically investigated the behavior of a diesel marine engine firing with ammonia–hydrogen blends and performing an HCCI combustion mode able to reduce the NO_X formation.

The state of the art demonstrates that engines fueled by ammonia–hydrogen are interesting due to their low environmental impact and good operating capacity.

Thus, in this paper, the operation of a light-duty spark-ignition engine fueled with an ammonia–hydrogen blend was investigated by means of a 1D numerical approach.

The blend was composed by 85% of ammonia and 15% of hydrogen by volume. It was chosen considering a previous literature analysis of these blends. In particular, a low amount of hydrogen, such as the one chosen in this work (15% by volume), could be directly produced on-board vehicles from an ammonia cracking process.

The analyses were performed taking into account the operating constraints of the engine. In particular, limits on the in-cylinder pressure, exhaust gas temperature, spark advance, knock intensity, and fraction of fuel burnt were considered. To the best of the authors' knowledge, previous studies do not show complete operating maps of a light-duty SI PFI engine fueled with the selected ammonia–hydrogen mixture. Therefore, the aim of this work was to assess both the performance and operating range of the engine, in order to obtain optimized engine maps which guaranteed its proper operation with the analyzed fuel blend.

2. Materials and Methods

With the aim of investigating the possible utilization of neat ammonia as a fuel for ICEs, the fueling change of a turbocharged gasoline engine, designed for light-duty vehicles, was analyzed (Section 2.1).

Engine performances were evaluated by using a numerical 1D model able to simulate the engine performances for different fuels (Section 2.2). The dependability of the 1D results strongly depended on a proper prediction of the in-cylinder pressure curves. The predicted in-cylinder pressure curves were compared to those obtained by a 3D numerical approach. The latter was based on a detailed chemical–kinetic mechanism able to predict the ammonia–hydrogen–air mixture oxidation (Section 2.3).

2.1. Engine and Fuel Blend

The engine under study is a PFI turbo-charged spark-ignition engine. It was designed to be fueled by regular gasoline. Some engine characteristics are shown in Table 2 which reports the nominal performances of the engine running with gasoline as designed by the manufacturer.

Table 2. Engine main characteristics for gasoline fueling.

Model	4 Cylinders, 4 Valves/cyl
Displacement (cm^3)	1368
Bore/Stroke/Con. Rod (mm)	72/84/129
Compression Ratio (-)	9.8
Combustion Chamber Shape	Pent Roof
Max Power (ISO Conditions) (kW)	110 @ 5500 rpm
Max Torque (ISO Conditions) (Nm)	230 @ 3000 rpm
Turbocharger group	IHI RHF3

In this work, the fuel system was modified in order to inject both ammonia and hydrogen fuels in the intake runners. In this way, the engine fired with a premixed hydrogen–ammonia–air mixture. In the following, the fuel was a blend of 85% ammonia and 15% hydrogen by volume. The main properties of the considered blend are summarized in Table 3.

Table 3. Fuel blend properties (ammonia 85%–hydrogen 15% by volume).

	Blend
LHV (MJ/kg)	33.98
Stoichiometric air to fuel ratio (-)	6.63
Heat released by a volume unit of stoichiometric air–fuel mixture (MJ/m^3)	2.82
Laminar burn velocity (m/s) in ambient condition *	0.088
Density (kg/m^3)	0.69

* Data calculated by Equation (1).

2.2. 1D Numerical Approach

A 1D model approach was used in order to evaluate the operation of the engine firing with ammonia–hydrogen blends. The model was already validated considering the engine running with gasoline [25] and different gasoline–alcohol blends [26]. The average error with respect to experimental data was less than 5% for fuel consumption, exhaust gas temperature, and maximum in-cylinder pressure. The same model was also used to predict the performance of the same engine fueled by hydrogen [6] or pure ammonia [12].

The numerical approach used for the combustion modeling decouples turbulence and chemical effects. Implementing the chemical properties of the ammonia–hydrogen–air mixture (laminar flame speed and induction time), since the kind of fuel does not affect the fluid dynamic behavior in a significant manner, the approach was still considered valid to predict the combustion process of the ammonia–hydrogen blend.

In Figure 1, the whole engine layout is presented. Briefly, the turbocharger was modeled by using the operation maps provided by the manufacturer, while in-pipe flow was estimated using a finite volume approach. The inlet air filter, which affects the performance and emissions of both spark-ignition engines [27] and compression ignition engines [28,29], was modeled as a volume. The friction losses were also considered according to data provided by the manufacturer.

The wastegate valve operation was simulated, allowing a portion of the exhaust gases to bypass the turbine. This was needed to control the boost pressure. The heat transfer rate through the cylinder walls was estimated using the well-known Woshni correlation. The friction losses were calculated as a function of the engine speed.

The injector was modeled considering a mixture with properties that nominally represent the fuel blend characteristics.

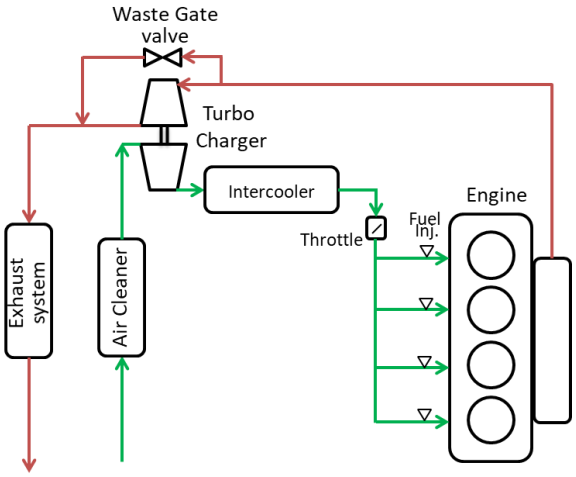

Figure 1. Schematic layout of the engine [20,27].

The burning rate for homogeneous charge spark-ignition engines in this model was predicted using the Keck and Tabaczynski model [30,31]. The calculated turbulent flame speed depended on both laminar flame speed and turbulent flow indices according to an entrainment model. Following the hierarchical approach described in [32], the mean turbulent length scale and the mean turbulent intensity were imposed, exploiting the flow field details provided by 3D calculations.

The thermochemical properties of the ammonia-hydrogen blend were utilized, while the laminar flame speed (S_L) was computed by means of the correlation presented in [33].

$$S_{L,NH3,H2} = S_{L0_2} * T_n^{\alpha_2} * P_n^{\beta_2} \quad (1)$$

$$\alpha_2 = a_{2,P_3} + b_{2,P_3} * \lambda + c_{2,P_3} * \lambda^2 + d_{2,P_3} * \lambda^3 \quad (2)$$

$$\beta_2 = a_{3,P_3} + b_{3,P_3} * \lambda + c_{3,P_3} * \lambda^2 \quad (3)$$

$$S_{L0_2} = a_1 * b_{1,P_4}^{\lambda} * \lambda^{c_{1,P_4}} \quad (4)$$

$$a_1 = a_{10} + (1 - a_{10}) * (1 - e^{-a_{11} * xH_2 - a_{12} * x^2 H_2 - a_{13} * x^3 H_2}) \quad (5)$$

where T_n and P_n are the normalized temperature and pressure with respect to the reference conditions of T and P, respectively, equal to 300 K and 0.1 MPa.

$$T_n = T_u / T_0 \quad (6)$$

$$P_n = P_u / P_0 \quad (7)$$

The coefficients a, b, c, and d are tabulated as a function of temperature and pressure in [33]. λ is the air to fuel ratio.

Figure 2 compares the calculated laminar flame speed of the hydrogen-enriched ammonia to those of pure ammonia and gasoline. It is worth noting that with a small amount of hydrogen, the laminar flame speed increased by 47.8% at an equivalence ratio equal to 1.

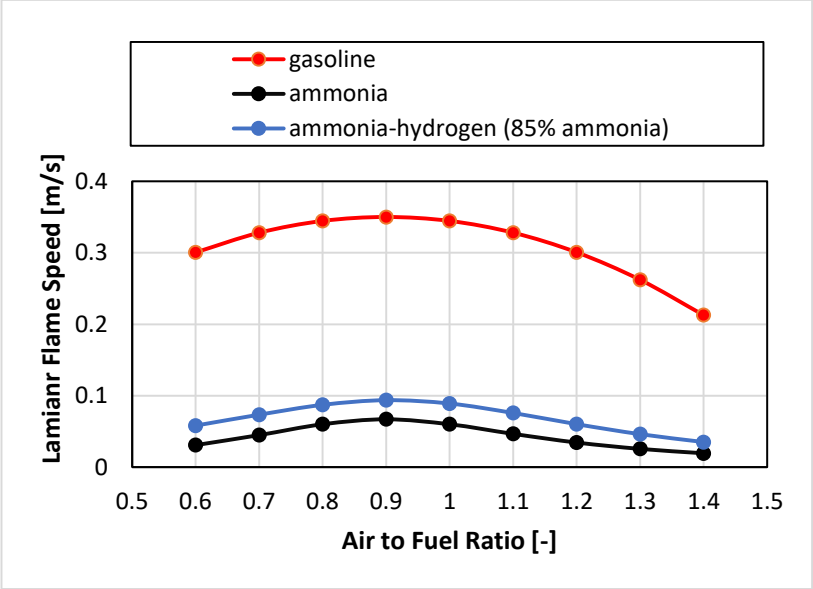

Figure 2. Laminar flame speed comparison in ambient condition. Data were calculated according to Equations (1)–(5) for ammonia and hydrogen–ammonia blend, according to [34] for gasoline.

The knock occurrence was detected considering the induction time of the air fuel mixture. It was assumed that knock occurs when $\int_0^t dt/\tau_{id}(t) = 1$ [35]. The ignition delays were provided by detailed chemical kinetic calculations previously performed in the Cantera environment [36]. In particular, the Nakamura mechanism [37], based on 38 species and 232 reactions, was solved in a "Ideal Gas Reactor" component. Several levels of pressure and temperature like those characterizing the engine operation were considered. The calculated data were tabulated, and the resulting database was implemented in the 1D model.

When knock is detected, its intensity is evaluated as described in the following equation:

$$KI = (1 - x_b)(cr - 1)\sqrt{1 - \frac{\theta_k}{\theta_{ref}}}\frac{N}{N_{ref}} \quad (8)$$

where x_b is the mass of burned fuel, cr is the compression ratio, θ_k is the knock onset crank angle and N the engine speed, and θ_{ref} is the maximum crank angle for which knock is still audible, set to 50 CAD. N_{ref} is a tuning parameter set as equal to 3500 rpm. It was assumed that tolerable knock corresponds to a KI level less than or equal to 0.5, as described in [12,25].

2.3. Three-Dimensional Numerical Approach

A 3D computational model, previously built by means of the commercial code AVL Fire, was used to reproduce some 1D results. Briefly, a first-order (Euler) implicit differencing scheme was used for time discretization, while second-order schemes were used for both continuity and momentum equations. An upwind scheme was used for both turbulence and energy equations. Turbulent effects were modeled using the well-known k-ε approach. This model was widely used in the past to reproduce the behavior of the same engine running with gasoline, obtaining very reliable results [32]. It was adapted to the ammonia–hydrogen engine operation referring to the Nakamura mechanism previously described. Thus, different chemical species were considered during the simulations, and the fuel oxidation process was simulated by means of a chemical–kinetic approach. The engine mesh, reported in Figure 3, reproduces only half geometry due to the symmetry of the engine geometry. The minimum number of the grid cells is about 50,000 (firing TDC), while the maximum number is approximately 350,000 (BDC during the intake stroke). Boundary

and initial conditions were set by utilizing the computations provided by the 1D model previously depicted. In the inlet runner, a premixed air–fuel mixture was considered.

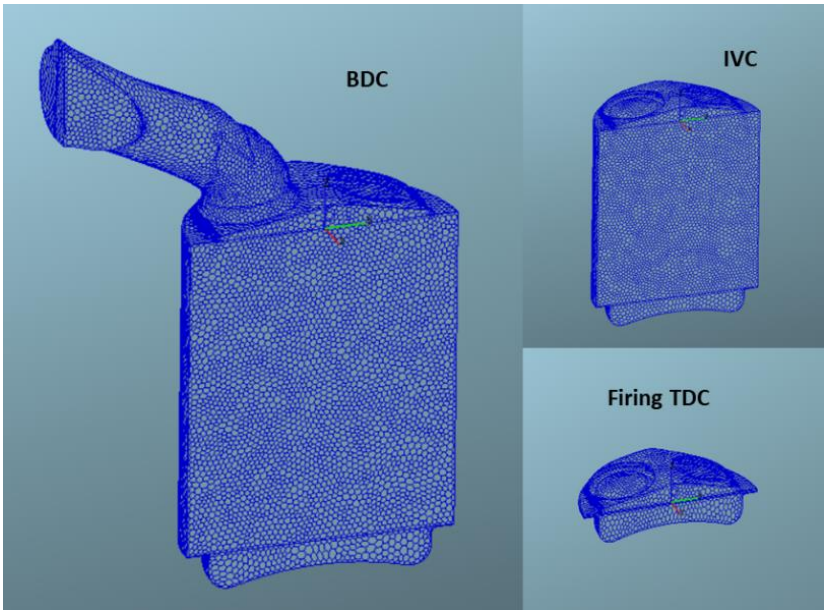

Figure 3. Three-dimensional engine mesh.

3. Results

The model described in Section 2.2 was used in order to evaluate the operation of the engine considering fueling with an ammonia–hydrogen blend. In particular, as already specified above, a blend of 85% ammonia and 15% hydrogen by volume was used.

Steady-state engine operating points in stoichiometric conditions were investigated. First, 3D computations were performed in order to investigate some operating points and to compare the 3D results with those obtained from the 1D computations (Section 3.1). In a second step, different analyses were carried out by using the 1D model in order to investigate both the performances and the operation limits of the engine fueled with the ammonia–hydrogen mixture.

The 1D simulation results are presented in the following. Low load operation was investigated considering no boost conditions and different values of the throttle opening (Section 3.2). Medium and high load operation was evaluated by varying the boost pressure at wide-open throttle (WOT) (Section 3.3).

In the end, taking into account several constraints which guarantee a proper operation of the engine (Table 4), the engine operating map is built in Section 3.4.

Table 4. Operating constraints.

Peak pressure (bar)	$\leq$100
Exhaust gas temperature (K)	$\leq$900
Spark advance (°bTDC)	$\leq$110
Knock intensity (-)	$\leq$0.5
Burned fuel fraction (%)	$\geq$98

The details of each analysis are described in the respective subsection.

3.1. 1D–3D Comparisons

The 3D approach was used to reproduce the WOT operating points presented in Table 5. The spark advance was chosen by means of the 1D simulation results aiming toward the maximum engine torque. It is worth noting that the spark advance values, as

discussed in [12] and [18], were bigger than the ones typical for the engine running with gasoline but were much lower than the values obtained for pure ammonia. As reported in Table 5, when increasing the engine speed, the spark advance moves far away from the top dead center (TDC).

Table 5. Three-dimensional simulated points. WOT.

Engine Speed	1500	3000
Spark advance (°bTDC)	54.4	64.3
Equivalence ratio (-)	1	1
Boost pressure (bar)	No boost	No boost

Figure 4 shows both in-cylinder pressure and heat release curves for each investigated case. The best agreement between the models was reached at 3000 rpm with a difference in pressure peak of about 0.47%, while at 1500 rpm, the difference was of about 4.9%. The agreement between the two models seemed to be good. These results confirm that the 1D model effectively predicted the behavior of the analyzed engine. Thus, it was implemented for the following analyses involving the fuel blend under study.

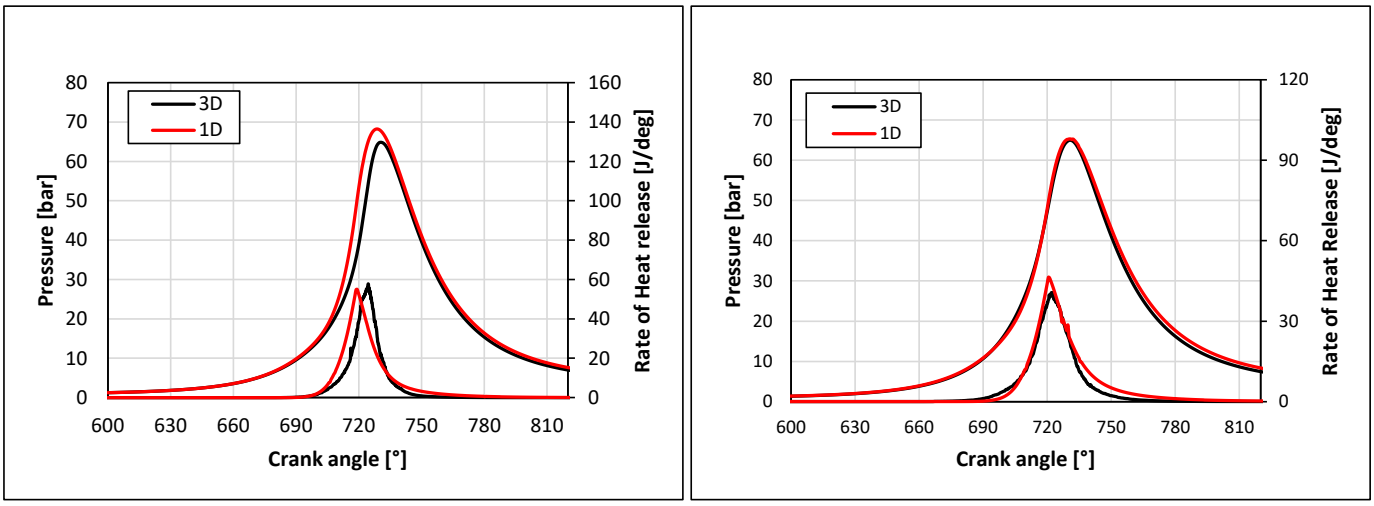

Figure 4. In-cylinder pressure and rate of heat release. The 1500 (**left**)–3000 (**right**) rpm, no boost, WOT.

3.2. Low Load Operation

In order to assess the engine behavior at partial load, a parametrical analysis was carried out by varying the throttle opening until a minimum torque of about 10 Nm was reached. The whole analysis was performed considering different engine speeds (from 1500 to 6000 rpm), no boost condition, an overall equivalence ratio equal to 1, and spark timing set to the maximum torque value.

As an example, Figure 5 shows the engine efficiency calculated at 3000 rpm when the load changes. Of course, due to the increasing pumping losses, when reducing the engine load by throttling, the efficiency decreased.

Furthermore, the typical increase in the angular combustion duration (CA 0–90) for increasing engine speeds (Figure 6, right) became critical for the lowest loads at medium regimes and for almost all the loads at high regimes. In fact, in the latter cases, the minimum allowable burned fuel fraction (98%) was not reached (Figure 6, left). As a consequence, the operating range of the engine significantly reduced. Partial load conditions were sustainable for the whole considered range at 1500 and 2000 rpm, with a burned fuel fraction at minimum load, respectively, equal to 98.8% and 98.9%. At 3000 and 4000 rpm, the entire map was not exploitable since the lowest loads did not respect the imposed constraint. At 5000 rpm, only WOT and very low throttling conditions guaranteed a proper

engine operation, while at 6000 rpm, the 98% burned fuel fraction was not reachable. It is worth underlining that, in this partial load analysis, all the other constraints were respected; therefore, they are not reported.

Engine running at 3000 rpm, no boost.

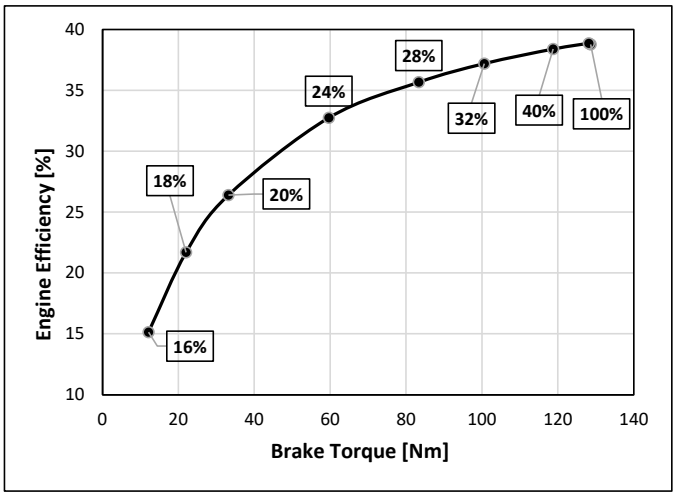

Figure 5. Engine efficiency as a function of engine torque for different throttle opening values.

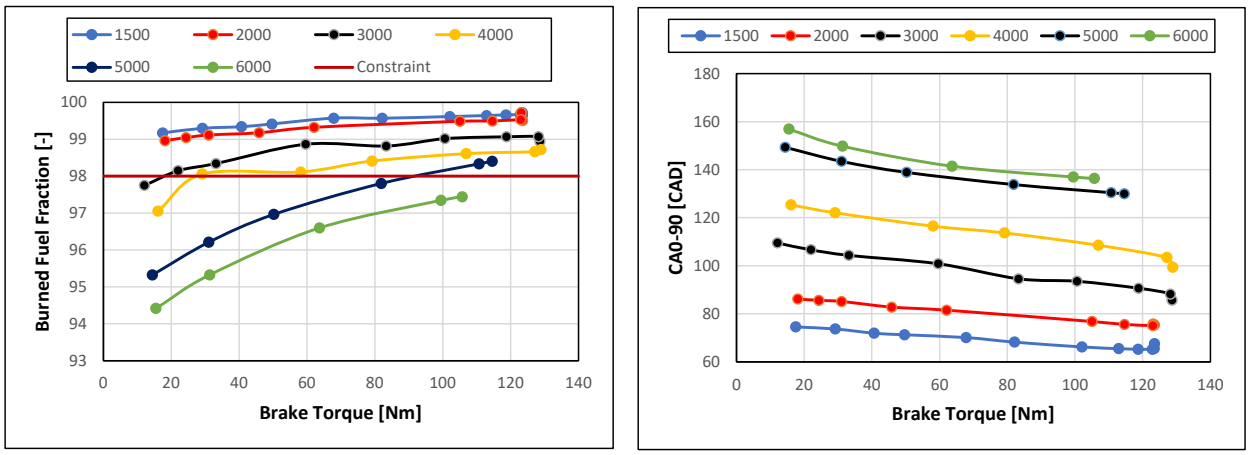

Figure 6. Burned fuel fraction (**left**) and CA 0–90 (**right**) for different regimes. No boost.

3.3. Medium and High Load Operation

In this subsection, the behavior of the engine at WOT was evaluated considering different engine speeds, from 1500 to 6000, and different boost pressure (BP) levels, up to 2 bar. Stoichiometric mixtures were always considered.

Figure 7 (left) shows the calculated engine torque delivered by the engine when the spark timing was set to the maximum torque knock limited value (Figure 7, middle). Of course, the engine torque increased when the boost pressure level grew. The optimal knock limited spark advance followed the trend of the combustion duration (Figure 7, right) which increased for increasing engine speeds and decreased when the boost pressure increased. It is worth noting that the combustion durations, presented in Figure 7 (right) for the speed of 1500 rpm, agreed with those measured in [18].

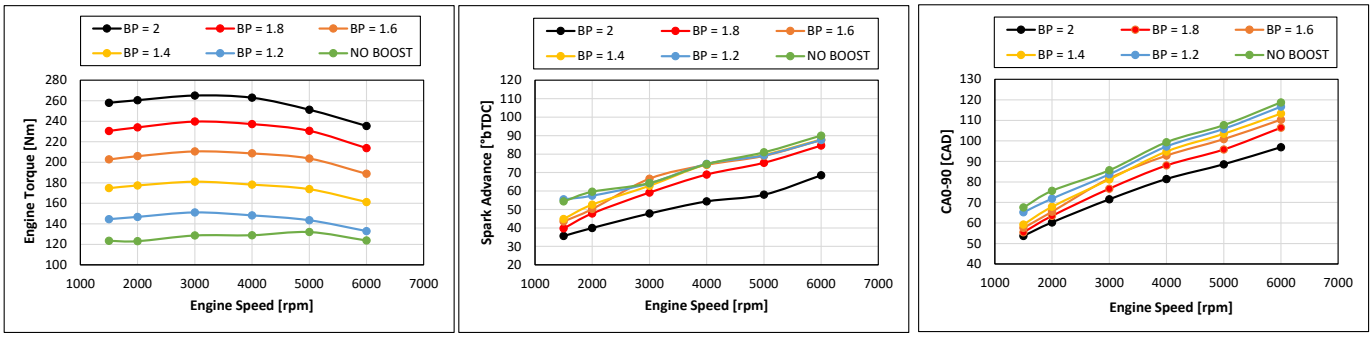

Figure 7. Engine torque (**left**) calculated at maximum torque knock limited spark advance (**middle**) and relative combustion duration (**right**) at different boost pressure levels.

Unfortunately, considering the operating constraints reported in Table 4, not all the points shown in Figure 7 were acceptable (Figure 8). The engine running with the optimal spark advance reached an unacceptable peak pressure for boost greater than or equal to 1.6 at any rotational speed. In addition, it reached unacceptable exhaust gas temperatures when it ran above 5000 rpm at any boost pressure levels. The exhaust gas temperature only did not limit the engine operation below 3000 rpm, while in the range of 3000–5000 rpm, it determined a maximum allowable boost pressure.

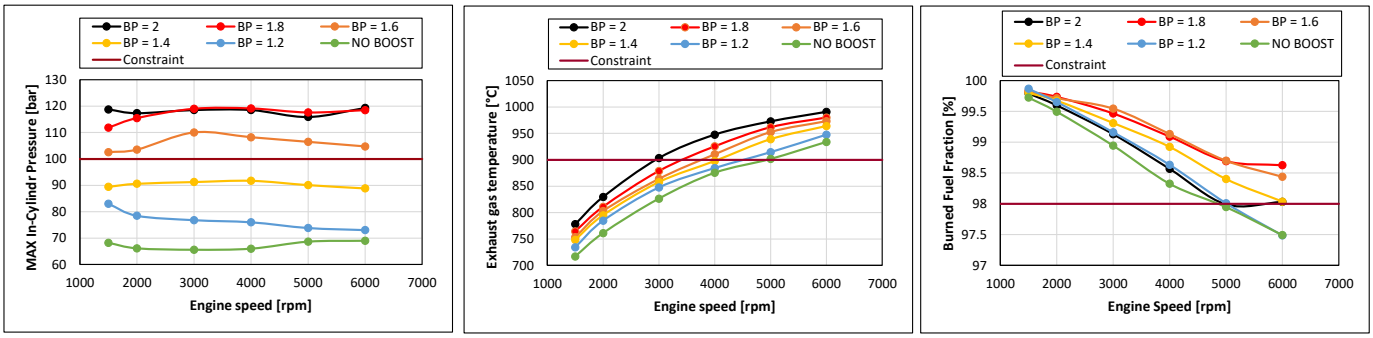

Figure 8. Maximum in-cylinder pressure (**left**), exhaust gas temperature (**middle**) and burned fuel fraction (**right**) calculated for the engine running at the maximum torque knock limited spark advance.

Finally, above 5000 rpm and at low boost pressure, the engine also showed unacceptable unburned fuel fractions at exhaust.

3.4. Engine Maps

The results reported in previous sections show that engine operation is strongly limited by the constraints reported in Table 4.

However, for some operating points, by varying the spark advance with respect to the optimal value, which guarantees the maximum torque, it is possible to extend the operating range of the engine. As an example, at 3000 rpm and a boost level equal to 1.6, and by delaying the spark time, the maximum pressure decreased until it became acceptable. Naturally, both exhaust gas temperature and unburned fuel fraction increased, but they still remained within allowable limits (Figure 9). This result was achieved and only lost about 3% of engine efficiency (Table 6).

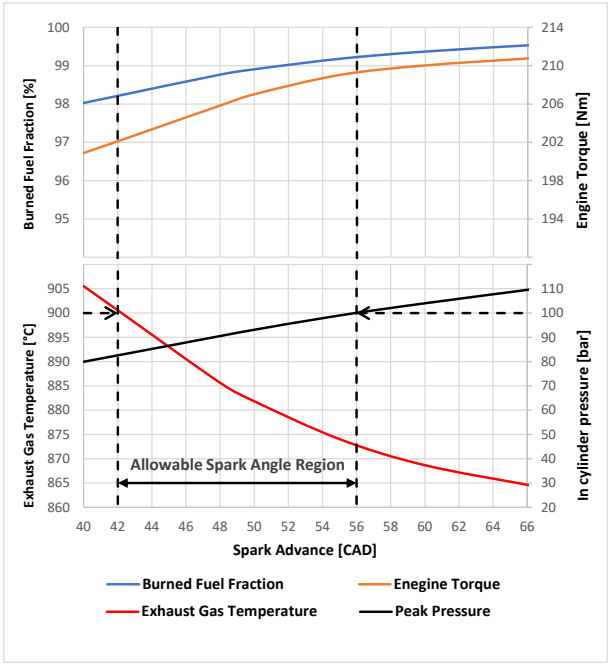

Figure 9. In-cylinder pressure, burned fuel fraction, exhaust gas temperature and engine torque versus spark advance. Engine speed: 3000 rpm, boost pressure: 1.6 bar. For this engine operating point, the maximum torque spark advance is 66.9 crank angle degrees, and the knock intensity is always zero. The allowable spark advance region is determined by constraints on the peak pressure and exhaust gas temperature.

Table 6. Engine recalibration at 3000 rpm, boost 1.6.

	Maximum Torque Operating Point	Recalibrated Operating Point
Max. In-Cylinder Pressure (bar)	101	89.9
Engine Torque (Nm)	212	210
Engine Power (kW)	66.5	65.9
Engine Efficiency (%)	41.4	40.0
Spark advance (°bTDC)	66.7	55.0
Exhaust Gas Temperature (°C)	869	874
Burned Fuel Fraction (%)	99.5	99.2

Thus, it is possible to identify an operating area where all parameters are within acceptable limits for many engine operating points that have been previously excluded.

The results of this constrained optimization are shown in Figure 10, where various engine parameters are represented as a function of engine speed and torque.

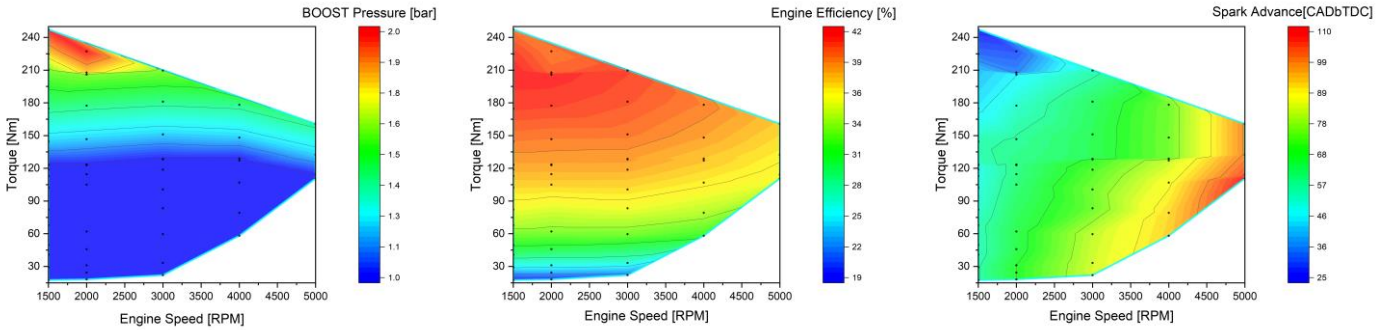

Figure 10. Boost level, engine efficiency, and spark advance as a function of engine speed and torque.

The feasible region was large enough at low engine speeds where good engine operation was possible. Between 1500 rpm and 3000 rpm, the engine could be regulated, delivering a torque ranging from a minimum value around 15 Nm to a maximum value greater than 200 Nm. The maximum engine torque was about 240 Nm; it was delivered at 1500 rpm, where a boost pressure equal to 2 bar could be achieved. This boost level could be kept only up to 2000 rpm.

Above 3000 rpm, the engine could run with an average maximum boost pressure of 1.4 bar, and the maximum delivered toque decreased almost linearly with the engine speed. In addition, the minimum load achievable by the engine decreased significantly as the engine speed increased. The combination of these two effects reduced the operating capacity of the engine as the speed increased. It could not run at 6000 rpm.

The engine efficiency was higher than 33% for almost all points; it never fell below about 19%. The maximum efficiency was very high: it was about 42% when the engine ran at low speed and the load was slightly less than the allowable maximum. Correspondingly, the specific consumption turned out to vary from about 350 g/kWh to about 750 g/kWh.

Spark advances are always very high. They ranged from a minimum of 25 CAD at 1500 rpm, maximum load, to a maximum of 110 CAD at 5000 rpm, low load.

4. Conclusions

In this paper, the authors investigated the behavior of a turbocharged spark-ignition light-duty engine powered by an ammonia–hydrogen blend (15% of hydrogen by volume) considering a port fuel injection. The analysis was carried out using a predictive 1D model. Furthermore, 3D computations were performed in order to verify the reliability of the results obtained by the 1D model.

The aim of the work was to assess both the performance and operating range of the engine in order to obtain optimized engine maps which guaranteed its proper operation with the chosen ammonia–hydrogen mixture.

The main results of the analysis can be summarized as:

- The small amount of hydrogen (by mass) improved the combustion behavior with respect to pure ammonia fueling, leading to reduced combustion durations and extending the operating range of the engine.
- Partial load operation became critical for the lowest loads at medium regimes and for almost all the loads at high regimes, due to unacceptable values of the burned fuel fraction. Low regimes (1500 and 2000 rpm) were sustainable for the whole considered throttling range. Medium regimes (3000 and 4000 rpm) were not sustainable at the lowest loads. At high regimes (5000 and 6000 rpm), a proper engine operation was not reachable, except for WOT and very low throttling conditions at 5000 rpm.
- At medium and high loads, the engine running with the optimal spark advance reached unacceptable values of the different constraints in various conditions, especially at the highest regimes (5000 and 6000 rpm) and at high boost levels (BP $\geq$ 1.6 bar). However, for some operating points, a specific tuning of the spark advance allowed all the operating constraints to be complied with (peak pressure, exhaust gas temperature, spark advance, knock intensity, and burned fuel fraction).
- Between 1500 rpm and 3000 rpm, the engine could be properly regulated. The engine could not reach 6000 rpm.
- At 1500 and 2000 rpm, the engine could reach a boost pressure equal to 2, while for the other regimes, the maximum feasible boost pressure was about 1.4.
- The maximum engine torque (about 240 Nm) was delivered at 1500 rpm. The engine efficiency ranged between 42% and 19%. Correspondingly, the specific consumption varied from about 350 g/kWh to about 750 g/kWh.

Author Contributions: Conceptualization, D.L. and E.G.; methodology, D.L., E.G. and G.D.; formal analysis, G.D., D.L. and E.G.; investigation, G.D.; data curation, G.D. and D.L.; writing—original draft preparation, G.D., D.L. and E.G.; writing—review and editing, G.D., D.L., E.G. and G.F.; supervision, E.G. and G.F. All authors have read and agreed to the published version of the manuscript.

Funding: This research received no external funding.

Data Availability Statement: Not applicable.

Conflicts of Interest: The authors declare no conflict of interest.

Nomenclature

1D	One-dimensional
3D	Three-dimensional
BDC	Bottom dead center
BP	Boost pressure
bTDC	Before top dead center
CA0–90	0–90% mass fraction fuel burn duration
CAD	Crank angle degree
COV_{IMEP}	Coefficient of variation of IMEP
HCCI	Homogeneous charge compression ignition
ICE	Internal combustion engine
IMEP	Indicated mean effective pressure
IVC	Intake valve closing
KI	Knock intensity
LHV	Lower heating value
NO_x	Nitrogen oxides
PFI	Port fuel injection
SI	Spark-ignition
TDC	Top dead center
WOT	Wide open throttle

References

1. Chiong, M.C.; Chong, C.T.; Ng, J.H.; Mashruk, S.; Chong, W.W.; Samiran, N.A.; Mong, G.R.; Valera-Medina, A. Advancements of combustion technologies in the ammonia-fuelled engines. *Energy Convers. Manag.* **2021**, *244*, 114460. [CrossRef]
2. Valera-Medina, H.A.; Xiao, M.; Owen-Jones, M.; David, W.I.; Bowen, P.J. Ammonia for power. *Prog. Energy Combust. Sci.* **2018**, *69*, 63–102. [CrossRef]
3. Tornatore, C.; Marchitto, L.; Sabia; de Joannon, M. Ammonia as Green Fuel in Internal Combustion Engines: State-of-the-Art and Future Perspectives. *Front. Mech. Eng.* **2022**, *8*, 944201. [CrossRef]
4. Ji, C.; Wang, S. Effect of hydrogen addition on combustion and emissions performance of a spark ignition gasoline engine at lean conditions. *Int. J. Hydrogen Energy* **2009**, *34*, 7823–7834. [CrossRef]
5. Fayaz, H.; Saidur, R.; Razali, N.; Anuar, F.; Saleman, A.; Islam, M. An overview of hydrogen as a vehicle fuel. *Renew. Sustain. Energy Rev.* **2012**, *6*, 5511–5528. [CrossRef]
6. Galloni, E.; Lanni, D.; Fontana, G.; D'Antuono, G.; Stabile, S. Performance estimation of a downsized SI engine running with hydrogen. *Energies* **2022**, *15*, 4744. [CrossRef]
7. Comotti, M.; Frigo, S. Hydrogen generation system for ammonia–hydrogen fuelled internal combustion engines. *Int. J. Hydrogen Energy* **2015**, *40*, 10673–10686. [CrossRef]
8. Kojima, Y.; Yamaguchi, M. Ammonia as a hydrogen energy carrier. *Int. J. Hydrogen Energy* **2022**, *47*, 22832–22839. [CrossRef]
9. CMørch, S.; Bjerre, A.; Gøttrup, M.; Sorenson, S.C.; Schramm, J. Ammonia/hydrogen mixtures in an SI-engine: Engine performance and analysis of a proposed fuel system. *Fuel* **2011**, *90*, 854–864. [CrossRef]
10. Onorati, A.; Payri, R.; Vaglieco, B.M.; Agarwal, A.K.; Bae, C.; Bruneaux, G.; Canakci, M.; Gavaises, M.; Günthner, M.; Hasse, C.; et al. The role of hydrogen for future internal combustion engines. *Int. J. Engine Res.* **2022**, *23*, 529–540. [CrossRef]
11. Xu, X.; Liu, E.; Zhu, N.; Liu, F.; Qian, F. Review of the Current Status of Ammonia-Blended Hydrogen Fuel Engine Development. *Energies* **2022**, *15*, 1023. [CrossRef]
12. Lanni, D.; Galloni, E.; Fontana, G.; D'Antuono, G. Assessment of the Operation of an SI Engine Fueled with Ammonia. *Energies* **2022**, *15*, 8583. [CrossRef]
13. Scharl, V.; Lackovic, T.; Sattelmayer, T. Characterization of ammonia spray combustion and mixture formation under high-pressure, direct injection conditions. *Fuel* **2023**, *333*, 126454. [CrossRef]
14. Cui, Z.; Tian, J.; Zhang, X.; Yin, S.; Long, W.; Song, H. Experimental Study of the Effects of Pre-Chamber Geometry on the Combustion Characteristics of an Ammonia/Air Pre-Mixture Ignited by a Jet Flame. *Processes* **2022**, *10*, 2102. [CrossRef]
15. El Fattah, S.F.A.; Ezzat, M.F.; Mourad, M.A.; Elkelawy, M.; Youssef, I.M. Experimental Investigation of the Performance and Exhaust Emissions of a Spark-Ignition Engine Operating with Different Proportional Blends of Gasoline and Water Ammonia Solution. *J. Eng. Res.* **2022**, *5*, 38–45.

16. Zhang, Z.; Long, W.; Dong, P.; Tian, H.; Tian, J.; Li, B.; Wang, Y. Performance characteristics of a two-stroke low speed engine applying ammonia/diesel dual direct injection strategy. *Fuel* **2023**, *332*, 126086. [CrossRef]
17. Zhang, H.; Li, G.; Long, Y.; Zhang, Z.; Wei, W.; Zhou, M.; Belal, B.Y. Numerical study on combustion and emission characteristics of a spark-ignition ammonia engine added with hydrogen-rich gas from exhaust-fuel reforming. *Fuel* **2023**, *332*, 125939. [CrossRef]
18. Lhuillier, C.; Brequigny; Contino, F.; Mounaïm-Rousselle, C. Experimental study on ammonia/hydrogen/air combustion in spark ignition engine conditions. *Fuel* **2020**, *269*, 117448. [CrossRef]
19. Frigo, S.; Gentili, R.; Doveri, N. Ammonia plus hydrogen as fuel in a SI engine: Experimental results. *SAE Tech. Pap.* **2012**. [CrossRef]
20. Wang, D.; Ji, C.; Wang, S.; Yang, J.; Wang, Z. Numerical study of the premixed ammonia-hydrogen combustion under engine-relevant conditions. *Int. J. Hydrogen Energy* **2021**, *46*, 2667–2683. [CrossRef]
21. Pyrc, M.; Gruca, M.; Tutak, W.; Jamrozik, A. Assessment of the co-combustion process of ammonia with hydrogen in a research VCR piston engine. *Int. J. Hydrogen Energy* **2022**, *48*, 2821–2834. [CrossRef]
22. Rodríguez, C.G.; Lamas, M.I.; Rodríguez, J.D.; Abbas, A. Possibilities of Ammonia as Both Fuel and NOx Reductant in Marine Engines: A Numerical Study. *J. Mar. Sci. Eng.* **2022**, *10*, 43. [CrossRef]
23. Liu, L.; Tan, F.; Wu, Z.; Wang, Y.; Liu, H. Comparison of the combustion and emission characteristics of NH_3/NH_4NO_2 and NH3/H2 in a two-stroke low speed marine engine. *Int. J. Hydrogen Energy* **2022**, *47*, 17778–17787. [CrossRef]
24. Wang, Y.; Zhou, X.; Liu, L. Theoretical investigation of the combustion performance of ammonia/hydrogen mixtures on a marine diesel engine. *Int. J. Hydrogen Energy* **2021**, *46*, 14805–14812. [CrossRef]
25. Lanni, D.; Galloni, E.; Fontana, G. Numerical analysis of the effects of port water injection in a downsized SI engine at partial and full load operation. *Appl. Therm. Eng.* **2022**, *205*, 118060. [CrossRef]
26. Scala, F.; Galloni, E.; Fontana, G. Numerical analysis of a downsized spark-ignition engine fueled by butanol/gasoline blends at part-load operation. *Appl. Therm. Eng.* **2016**, *102*, 383–390. [CrossRef]
27. Abdullah, N.R.; Shahruddin, N.S.; Mamat, A.M.I.; Kasolang, S.; Zulkifli, A.; Mamat, R. Effects of Air Intake Pressure to the Fuel Economy and Exhaust Emissions on a Small SI Engine. *Procedia Eng.* **2013**, *68*, 278–284. [CrossRef]
28. Dziubak, T.; Karczewski, M. Experimental Study of the Effect of Air Filter Pressure Drop on Internal Combustion Engine Performance. *Energies* **2022**, *15*, 3285. [CrossRef]
29. Dziubak, T.; Karczewski, M. Experimental Studies of the Effect of Air Filter Pressure Drop on the Composition and Emission Changes of a Compression Ignition Internal Combustion Engine. *Energies* **2022**, *15*, 4815. [CrossRef]
30. Metghalchi, M.; Keck, J.C. Burning velocities of mixtures of air with methanol, isooctane, and indolene at high pressure and temperature. *Combust. Flame* **1982**, *48*, 191–210. [CrossRef]
31. Metghalchi, M.; Keck, J.C. Laminar burning velocity of propane-air mixtures at high temperature and pressure. *Combust. Flame* **1980**, *38*, 143–154. [CrossRef]
32. Bozza, F.; Fontana, G.; Galloni, E.; Torella, E. 3D-1D analyses of the turbulent flow field, burning speed and knock occurrence in a turbocharged SI engine. *SAE Trans.* **2007**, *116*, 1495–1507.
33. Goldmann, A.; Dinkelacker, F. Approximation of laminar flame characteristics on premixed ammonia/hydrogen/nitrogen/air mixtures at elevated temperatures and pressures. *Fuel* **2018**, *224*, 366–378. [CrossRef]
34. Heywood, J.B. *Combustion Engine Fundamentals*, 1st ed.; McGraw-Hill Education: New York, NY, USA, 1988; Volume 25, pp. 1117–1128.
35. Livengood, J.; Wu, P.C. Correlation of Autoignition Phenomena in Internal Combustion Engines and Rapid Compression Machines. In Proceedings of the 5th Symposium (International) on Combustion, Pittsburg, PA, USA, 30 September–3 October 1955.
36. Goodwin, D.G.; Moffat, H.K.; Speth, R.L. *Cantera: An Object-Oriented Software Toolkit for Chemical Kinetics, Thermodynamics, and Transport Processes, Version 2.2. 1.*; Cantera Developers: Warrenville, IL, USA, 2017.
37. Nakamura, H.; Hasegawa, S.; Tezuka, T. Kinetic modeling of ammonia/air weak flames in a micro flow reactor with a controlled temperature profile. *Combust. Flame* **2017**, *185*, 16–27. [CrossRef]